

# Characterization of defects and graphite types in ductile cast iron by image processing and its relation to mechanical properties

V. Vokál\*, K.-F. Nilsson, P. Minnebo

*Institute for Energy JRC, Post Office Box 2, NL-1755 ZG Petten, Netherlands*

Received 14 June 2007, received in revised form 15 October 2007, accepted 18 October 2007

## Abstract

The paper presents a fast and reliable image processing tool to characterize graphite nodules and casting defects in ductile cast iron (IAOGT – Image Analysis of Graphite Types). Relationship between ductility of ductile cast iron and size of casting defects and different characteristic nodule properties (graphite type, feret, nodularity and nodule count) are indicated by analysis of 33 tested tensile specimens. The casting defects and variation in nodule properties interact in a complex way but casting defects in the form of oxide films contribute most to low ductility. Low nodularity, low nodule count and high feret of Graphite Type III, IV-V also reduce ductility.

**Key words:** ductile cast iron, graphite types, casting defects, ductility, image analysis

## 1. Introduction

Cast iron has been used for technical applications for many centuries. This class of ferrous alloys can be used for casting large components as they tend to show low melting temperatures, are very fluid when molten, do not form surface films when poured and undergo low amounts of shrinkage during solidification and cooling. The carbon in grey and ductile cast iron largely solidifies as free graphite with different shapes. In grey cast iron graphite flakes are formed that act as stress concentrators and crack initiation sites, which makes grey cast iron brittle. In ductile cast iron, which was invented six decades ago, a small amount of magnesium, sodium or cerium are added during the casting process whereby the graphite takes a more spherical shape, which significantly improves the ductility. Ductile cast iron has many applications such as automotive components, heavy machinery and wind energy turbines. It is also used for casks for radioactive waste and spent nuclear fuel, for instance the CASTOR<sup>®</sup> casks for transport and storage and the KBS-3 copper/cast iron canisters for long-term geological disposal of spent fuel that are being developed in Sweden and Finland [1] (Fig. 1).

The microstructure of ductile cast iron is quite

complex. In addition to variation in the size, number and shape of the graphite nodules, various casting defects such as blowholes, inclusions and oxide-compound films may be present. Ductile cast iron has therefore an inherent scatter in its material properties that one would like to minimize, but which cannot be completely eliminated. In applications for containing radioactive waste and spent nuclear fuel this becomes particularly important since the probability for failure, although at an extremely low value, can be sensitive to large scatter in material properties. A three-year research project between the Swedish nuclear waste management organization, SKB, the European Commission's Joint Research Centre Institute of Energy and other Swedish organizations was undertaken. The objectives were firstly to demonstrate that the failure probability for the KBS-3 canisters remains extremely low even for the isostatic pressure loads during future ice ages, and secondly to outline associated acceptance criteria for defects, material properties and geometry tolerances for the ductile cast iron inserts [2], [3]. The project used results from a statistically based material characterization programme, where tension, compression and fracture tests were performed on specimens taken from the top and bottom of three different inserts. The most important conclusion was that the

\*Corresponding author: [vratko@vokal.name](mailto:vratko@vokal.name)

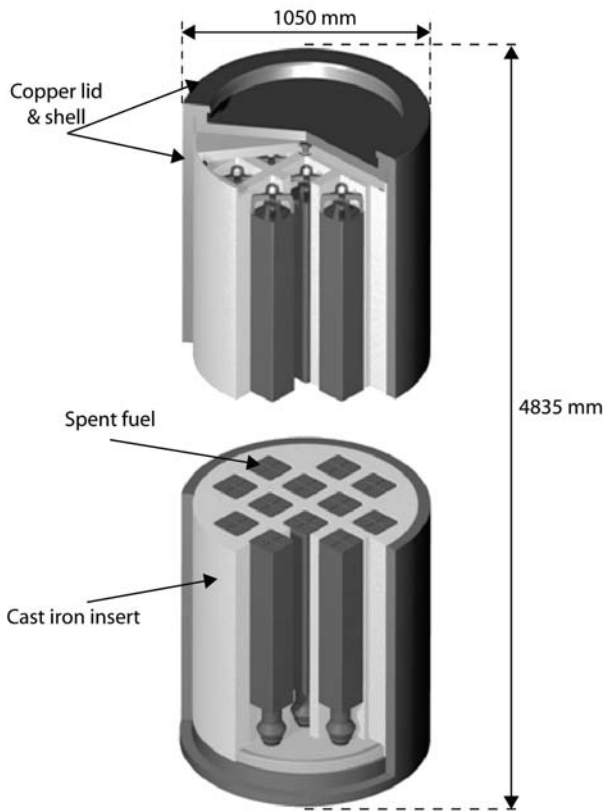


Fig. 1. The Swedish KBS-3 copper/cast iron canister for spent fuel.

failure probabilities were extremely low [3] (of the order  $10^{-8}$  per canister) provided certain geometry requirements were met. Nevertheless, the tensile ductility of the ductile cast iron was relatively low (in some cases below 2 %) compared to the initial standard material requirement of 11 % and there was significant scatter between specimens taken from different inserts and locations. Microstructural analyses showed that ductility values below 6 % were primarily caused by oxide film defects and to a smaller extent by high pearlite content [4], [5]. The reduction in ductility due to the oxide films was successfully modelled using elasto-plastic probabilistic fracture mechanics [5]. The graphite properties contributed to the low ductility values as well and it was conjectured that the variation in these controlled the ductility at values above 6 %.

In order to better understand the scatter in ductility in ductile cast iron and to more accurately model its properties the influence of the graphite properties (nodularity, shape parameters and number of nodules) needs to be analysed in more detail. The basis for this is a systematic and quantitative characterization of the various forms of graphite present in the microstructure. There are at least two problems to conduct such a characterization. Firstly it is quite

time consuming. Secondly, the judgement of the analyst often leads to a certain subjectivity of the results. This paper presents a microstructural analysis of 33 ductile cast iron specimens from the KBS-3 project mentioned above. The emphasis is on specimens with higher ductility values in order to assess the influence of the graphite variation. For each specimen a small segment was taken out from a location close to the fracture surface and analysed with respect to graphite properties. The casting defects are expected to play a role also for the specimens investigated here. Analysis of casting defects on fracture surfaces was therefore performed for each specimen to separate the effect of casting defects from the graphite variation. An image processing analysis tool was developed to reduce the analysis time and eliminate subjectivity of the results. In the previous study the sizing of casting defects and the categorization of the graphite nodules were done manually. Graphite properties and casting defects are quantified more accurately in the present study compared to the previous ones; the previous data were therefore not re-used in this study.

## 2. Experimental procedure

The joint SKB-JRC project used specimens from three different inserts referred to as I24, I25 and I26. The total number of tensile specimens was 153. The majority of the tensile specimens had a diameter of 14 mm, but there were also specimens with a 9 mm and 20 mm diameter. The I26 insert had higher pearlite content than I24 and I25, which contributed to its reduction in ductility. In the current study 33 specimens were investigated from insert I24 and I25. The material is ductile cast iron grade EN-GJS-400-15U, in accordance with the European standard EN 1563 [6]. By definition grade EN-GJS-400-15U is a cast ferrous material in which the free graphite is in a spherical form (nodular graphite GT-VI, in the ISO-standard ISO 945 graphite types are defined by representative pictures, Fig. 2 [7]). The chemical compositions of the material used in the two inserts are given in Table 1. For each insert, tensile test specimens were taken out from two different slabs: one cut from the top region of the insert and one removed from the bottom. The tensile tests were carried out in accordance with the European standard EN10002-1 [8]. A complete stress-strain curve was recorded for each specimen. Figure 3 shows a broken specimen with a segment cut out for microstructural analysis. Figure 4 shows histograms of the tested specimens as a function of tensile failure strain, indicating the subset selected for microstructural analysis in the earlier study where the emphasis was on casting defects found on the fracture surface, and the present one where the emphasis is on the graphite nodules.

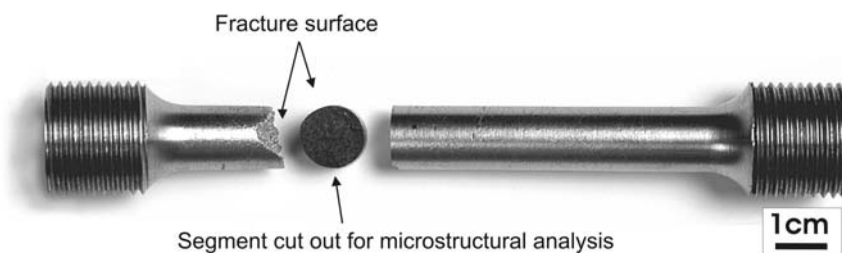


Fig. 3. A broken tensile specimen with a segment cut out for microstructural analysis.

Table 1. Chemical analysis of ductile cast iron inserts I24, I25

Insert	C (wt.%)	Si (wt.%)	Mn (wt.%)	P (wt.%)	S (wt.%)	Cr (wt.%)	Ni (wt.%)	Mo (wt.%)	Cu (wt.%)	Mg (wt.%)
I24	3.66	2.31	0.15	0.03	0.01	0.03	0.27	0.01	0.11	0.05
I25	3.78	2.08	0.21	0.01	0.01	0.04	0.50	–	–	0.04

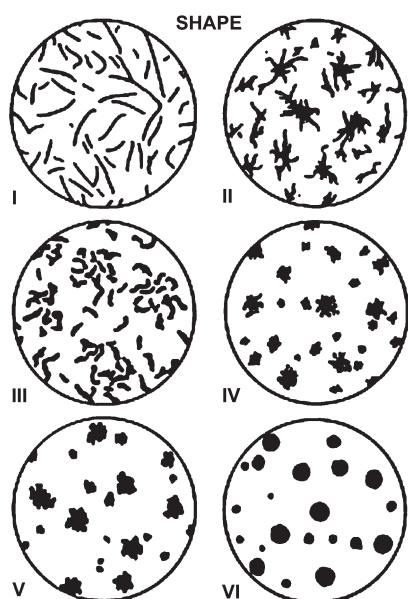


Fig. 2. ISO Graphite Types I to VI in cast iron according to ISO 945 [7].

Figure 5 shows the steps in the microstructural analysis. Segments with thickness of 10 mm were taken from the selected specimens from a section at 5 mm below the fracture surface (Fig. 3). The cut-out segments were subsequently embedded in resin, ground using SiC up to 1200 grid and then polished using 16 μm, 9 μm, 3 μm and 1 μm diamond suspensions. The microstructure of the samples was revealed by etching in 10 % Nital (10 % HNO<sub>3</sub> solution in ethanol) for about 10 seconds and recorded by high-resolution scanning electron microscope (SUPRA 50 LEO, at 15 kV, back-scattered electrons imaging (BEI) mode). The image analysis of graphite parameters was done

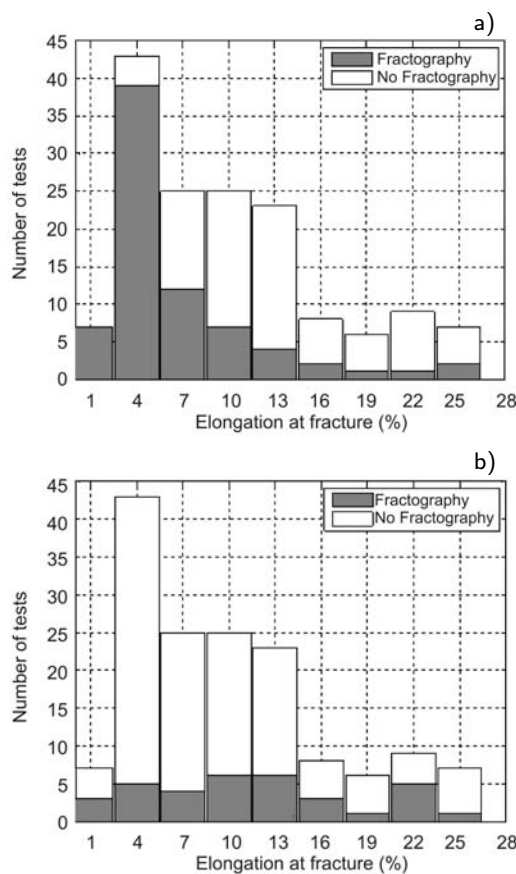


Fig. 4. Number of specimens investigated per ductility level by microstructural analysis showing a) subset in previous investigations [1–4] and b) subset in this investigation.

with a user-developed programme (IAOGT), which uses routines from the MATLAB<sup>1</sup> image processing

<sup>1</sup> MATLAB is a high-level language and interactive environment for numerical computations and with Toolboxes

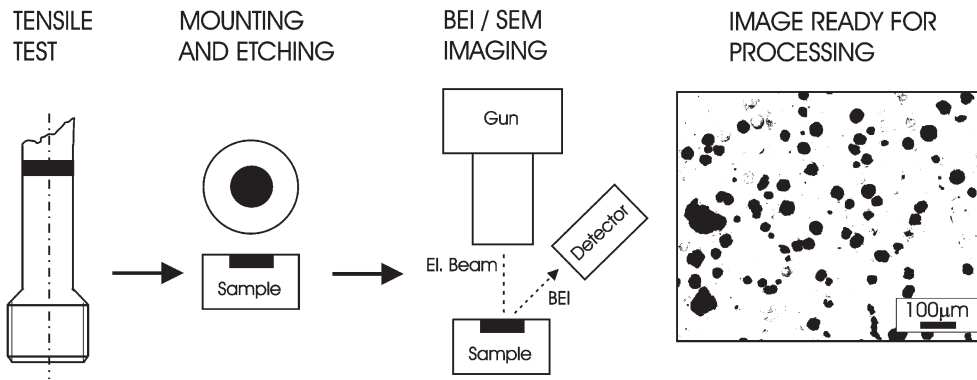


Fig. 5. Schematic of the sample handling and imaging process.

Toolbox. In this the graphite characterization is based on the modified approach presented by Velichko and Mucklich [9] and covers Graphite Types (GT) I, III, IV-V and VI in accordance with ISO 945 [7]. The details of the implementation are described in more detail in the following section.

The fracture surfaces of the selected specimens were also investigated. The fractographic analysis focused on casting defects since the previous studies indicated these as the main contributors to low ductility. The same scanning electron microscope was used for characterization at different magnifications. The Secondary Electrons Imaging (SEI) mode was used in order to reveal the surface morphology. Back-scattered Electrons Imaging (BEI) mode was used to identify matrix, graphite, secondary phases, inclusions and impurities. X-ray dispersive analysis (EDS) was also carried out to qualitatively investigate the chemical composition of casting defects.

### 3. The image processing tool

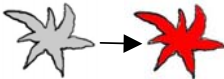
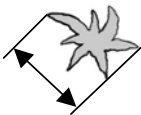
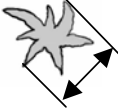




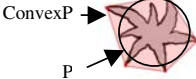
The free graphite was characterized for each specimen from a large number of micrographs (typically 20), each with approximately 100 nodules/image. This was done in accordance with ISO 945, using the following shape/region parameters: *Area*, *Maximum Feret*, *Minimum Feret*, *ConvexHull*, *ConvexP*, *Convex Image*, *Roundness* and *Compactness*. The definition of these parameters is given in Table 2. The shape/region parameters are determined for every region of each micrograph using the MATLAB Image Process routine 'regionprops'. The computed roundness and compactness of individual nodules are then mapped on a roundness/compactness plot. Figure 6a shows the results for all nodules for a representative specimen. The shape of two representative nodules with high and low roundness and compactness is in-

dicated. The graphite type for a nodule is determined from the value of these parameters as follows. For a quantitative classification, the different graphite types are defined by rectangular regions in the roundness-compactness plane. Figure 6b shows the graphite type regions as defined by Velichko and Mucklich [9]. From this it follows that a specific nodule may be classified as:

- a) clearly belonging to one of the regions, and in that case it will be assigned to the class of lamellar (GT I), vermicular (GT III), IV-V or nodular (GT VI) graphite, respectively;
- b) falling within the overlapping range of two identification domains in which case it will be assigned to both classes;
- c) if it does not fall within either of the above identification domains, then it does not belong to any of the four graphite types as indicated by the arrows (A) in Fig. 6b;
- d) if a graphite nodule is located on the boundary of examined image it is excluded from calculation as it gives faulty shape properties.

Nodule count (number of nodules per  $\text{mm}^2$ ) and nodularity are more often used than graphite types to characterize ductile cast iron. Nodularity is defined as the area of Graphite Type VI normalized with the total area of graphite, and may range from 0 to 100%. The overlapping regions in the GT definitions are a problem for computation of nodularity since a nodule may be counted twice. The case when a nodule does not fall into any of the GT regions is also not ideal since it is then not counted at all. It is therefore beneficial to minimize the number of nodules that are counted twice or not counted, even at the cost of not exactly fulfilling Velichko and Mucklich's criteria. An alternative definition of the GT regions shown in Fig. 6c was therefore adopted. The size, number and distribution of nodules of a specific graphite type are computed automatically by the IAOGT programme. Figure 7a shows a recorded image with all nodules in a specific region and Fig. 7b shows processed images isolating nodules of Graphite Types III, IV-V and VI.

Table 2. Description of parameters used for image analysis processing tool

Parameter	Description	Scheme
Area	The actual number of pixels in the region (nodule).	
Maximum feret	The length (in pixels) of the major axis of the ellipse that has the same normalized second central moments as the region (nodule).	
Minimum feret	The length (in pixels) of the minor axis of the ellipse that has the same normalized second central moments as the region (nodule).	
ConvexHull	The smallest convex polygon that can contain the region (nodule).	
ConvexImage	The convex hull, with all pixels within the hull filled in (i.e., set to on).	
ConvexP	The perimeter length of region taken from the ConvexImage.	
Roundness	The relation between area of the region and the area of a circle with same diameter as the region's Maximum feret calculated as: $R = A/A_{MF} = [4\pi A / (PI(\text{MaxFeret})^2)]$	
Compactness	Compares Area of the region (nodule) to the Area of the circle with the same perimeter as perimeter ConvexP (i.e. perimeter of smallest polygon round the region (nodule)). $C = A/A_{convP} = [4\pi A / (\text{ConvexP})^2]$	

By application of the procedure outlined above, the graphite type, nodularity or nodule count can be determined in a very fast and objective manner from the micrographs.

#### 4. Results

The tensile specimens' cross-sections and fracture surfaces were investigated using the procedure outlined above.

The fracture surface consisted of embedded nodular Graphite Type VI as well as free graphite precipitated as Graphite Types IV-V and III. The proportion of the different graphite types varied between specimens. Graphite Type I could not be unambiguously identified on fracture surfaces. Figure 5 suggests that this graphite type was identified on cross-sections but due to its shape it is almost impossible

to distinguish it from other casting defects on fracture surface. The fracture surfaces also contained different types of casting defects of varying sizes. In-situ forming oxide films of type  $(\text{Mg-Si-Fe})_x\text{O}_y$ , as shown in Fig. 8, form metallic and non-metallic inclusions which are characterized as G111, G121, G142 as defined in [10] were detected on many fracture surfaces. Blowholes, occasionally covered by thin graphite films, as shown in Fig. 9, were also detected on the fracture surfaces. The fracture surface macrographs were analysed using image processing tool IAOGT to determine the size and shape of the casting defects. Figure 10 shows macrographs of two specimens with low elongation at fracture probably caused by the casting defects. Figures 10a,b show the SEI macrograph of a fracture surface with many relatively small defects; these can be clearly seen on the processed images used in the IAOGT. A specimen with a large casting defect is shown in Figs. 10c,d.

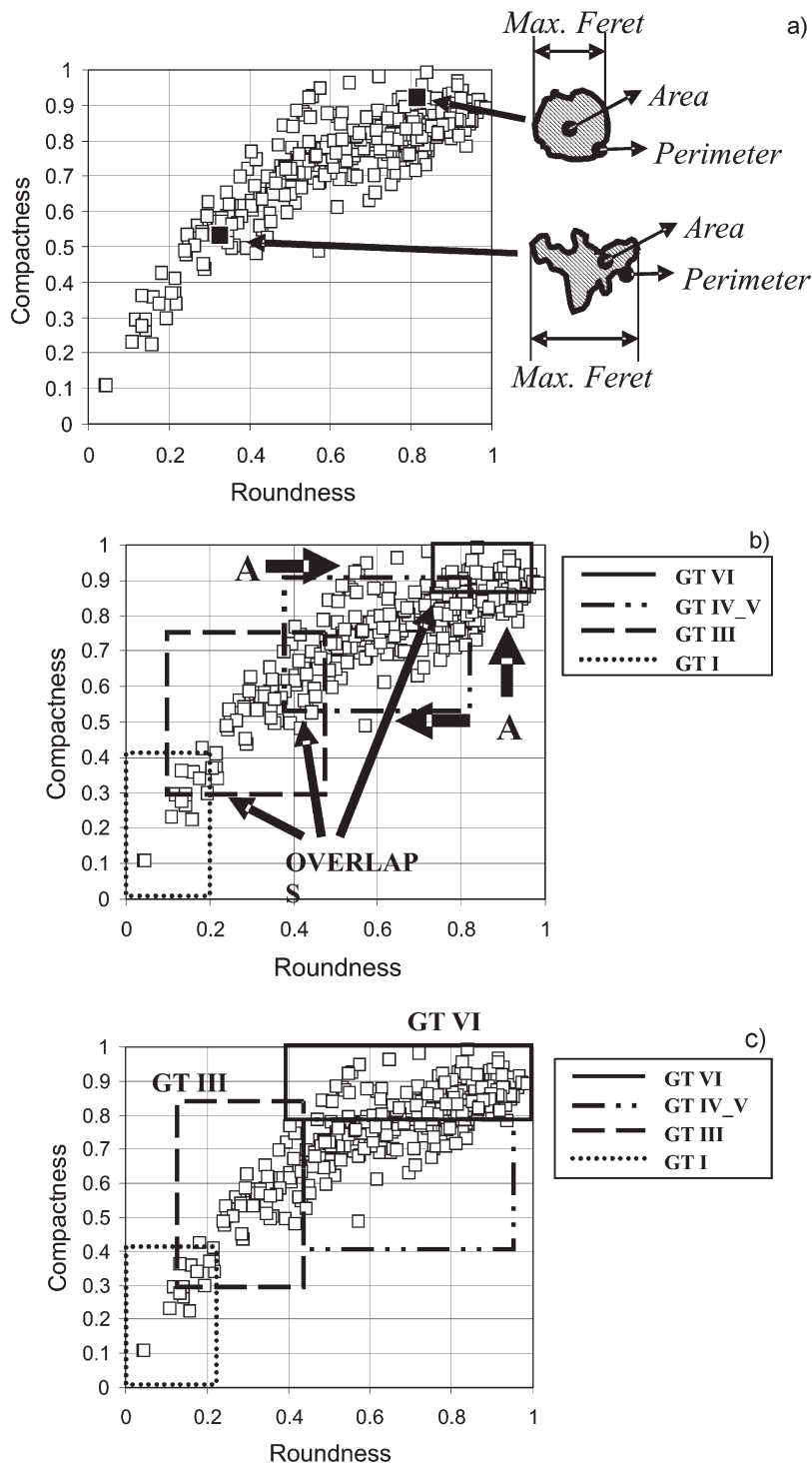


Fig. 6. Compactness and roundness from nodules measured for a single specimen using the image processing tool IAOGT: a) raw data points, b) regions for graphite types following the Velichko and Mucklich definitions, c) regions for graphite types with the alternative definitions used in this paper.

The elongation at fracture versus the measured maximum feret of the casting defects (oxide or graphite film) and the area fraction of the casting defects is shown in Figs. 11a,b, respectively. As has been observed in previous studies, the defect size has a significant role in reducing the ductility. The specimens

with maximum defect size larger than 1 mm are represented by open and filled symbols corresponding to nodule count higher and lower than  $100/\text{mm}^2$ , respectively. To study the effect of the graphite nodules, specimens with large defects should be excluded. Figures 12a,b show the elongation at fracture versus the size

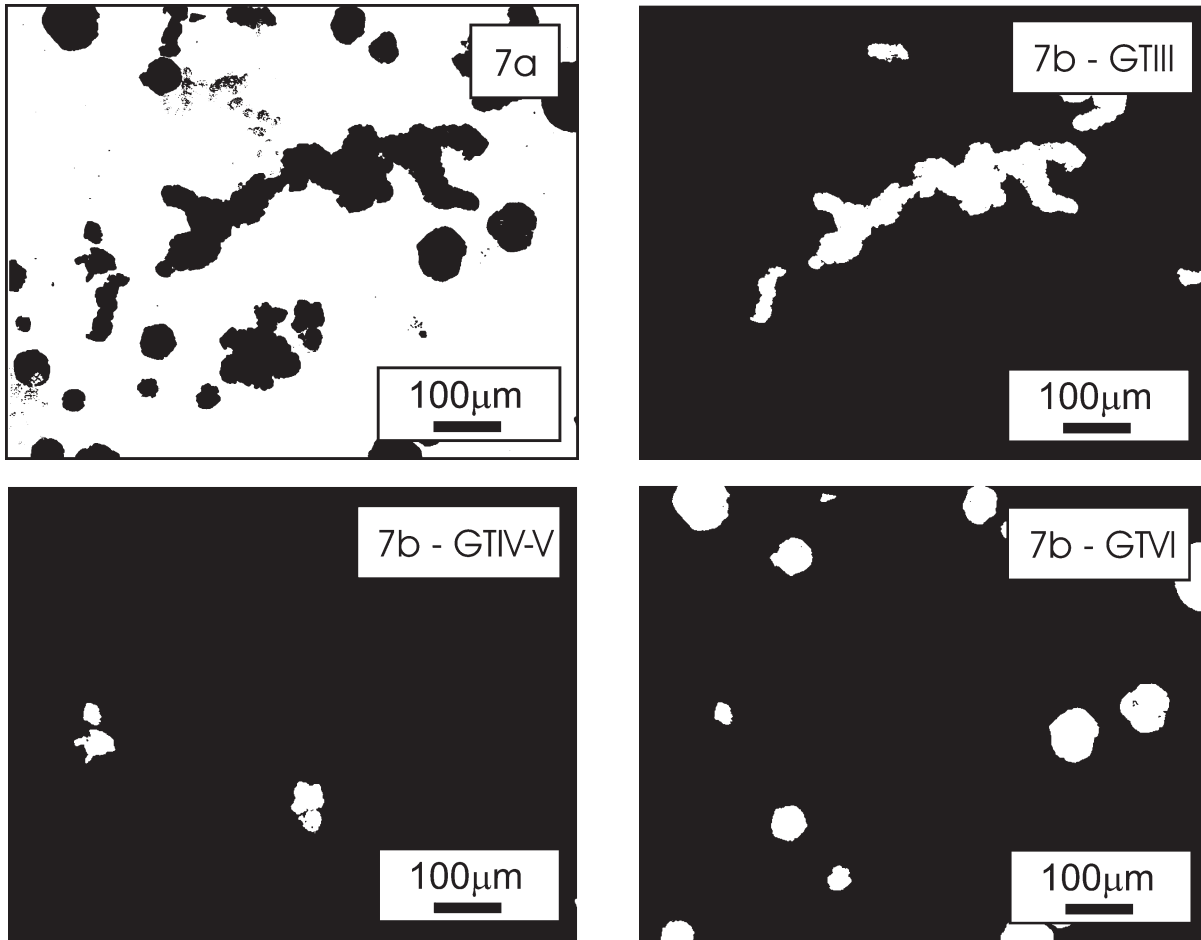


Fig. 7. Example of IAOGT (image software) output for GT IV-V: a) recorded image, b) processed image with GT III, GT IV-V and GT VI graphite types.

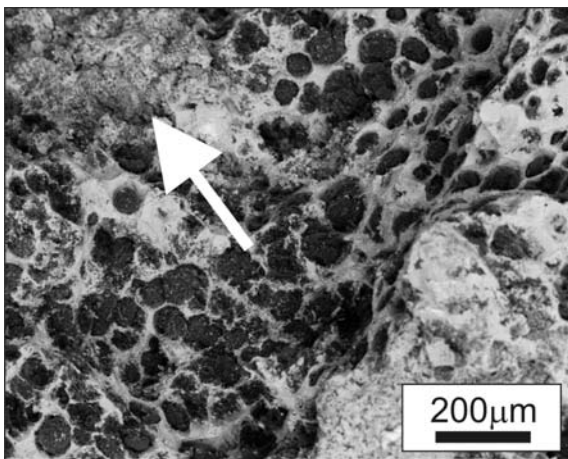


Fig. 8. SEM image of the fracture surface of a DCI specimen; the arrow indicates the Mg-Si-Fe Oxide Film. Nodular graphite (GT VI) is embedded in the surrounding ferritic matrix.

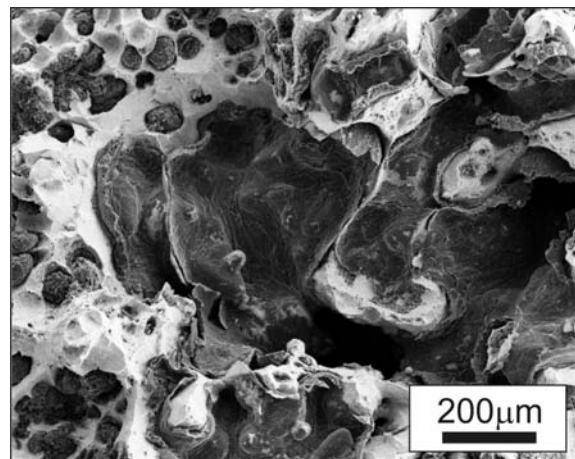


Fig. 9. SEM image of the fracture surface of a DCI specimen showing a thin graphite film covering the surface of a blowhole.

of maximum feret for GT III and GT IV-V nodules, respectively, that had been measured on the cross-

-sections and computed by the IAOGT software for the specimens with a maximum casting defect smaller than 1 mm on its fracture surface. There appears

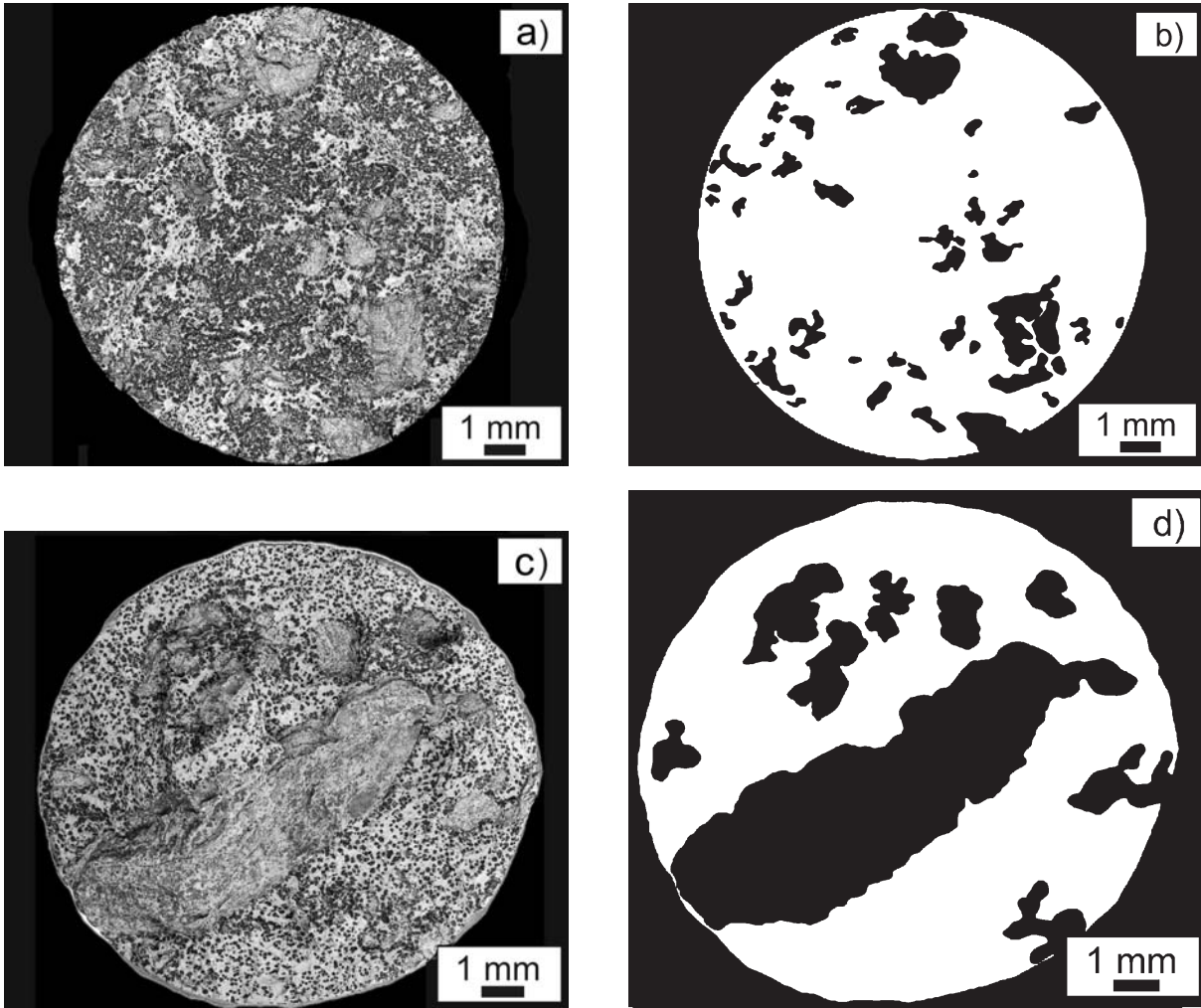


Fig. 10. Fracture surfaces with casting defects for two inserts (I24T6: specimen diameter 14 mm,  $A = 2.3\%$ ) and (I24LS3: specimen diameter = 9 mm,  $A = 1.4\%$ ): a) SEI-macrograph of I24T6, b) processed picture for defect sizing of I24T6, c) SEI-macrograph of I24LS3, d) processed picture for sizing defects of I24LS3.

to be a clear trend that the ductility decreases with the maximum feret for these two graphite types. The linear trends are:

$$\begin{aligned} A_{GTIII} &= -0.0224 \cdot GTIII_{\text{MaxFeret}} + 23.2, \\ A_{GTIV-V} &= -0.064 \cdot GTIV - V_{\text{MaxFeret}} + 27.3. \end{aligned} \quad (1)$$

Figures 13a,b show respectively the measured elongation at fracture versus the computed nodularity and nodule count for the investigated specimens. From the data with small casting defects it is quite obvious that elongation at fracture increases with increasing nodularity. A small number of nodules also seem to have a negative effect on the elongation at fracture. This is more clearly shown by the filled symbols in Fig. 13a than in Fig. 13b. It should be remembered though that the results are influenced by the variation in defect size. The empirical trend curves shown in the plot for the elongation at fracture versus nodularity

and nodule count for the specimens with small defect size are:

$$\begin{aligned} A_{\text{Nodularity}} &= 6.51 \cdot e^{0.02 \cdot \text{Nodularity}}, \\ A_{\text{NoduleCount}} &= 0.0283 \cdot \text{NoduleCount} + 12.6. \end{aligned} \quad (2)$$

An exponential fit has been used for the nodularity since there is a clear upwards shift.

## 5. Discussion

The results presented in this paper and the previous studies clearly show that oxide film defects lower the ductility of ductile cast iron. The ductility is also affected by variation in the graphite nodules shape. The detrimental effect of maximum feret for Graphite Type III and IV-V was indicated in this paper. The ideal graphite structure has high nodularity and high nodule count.



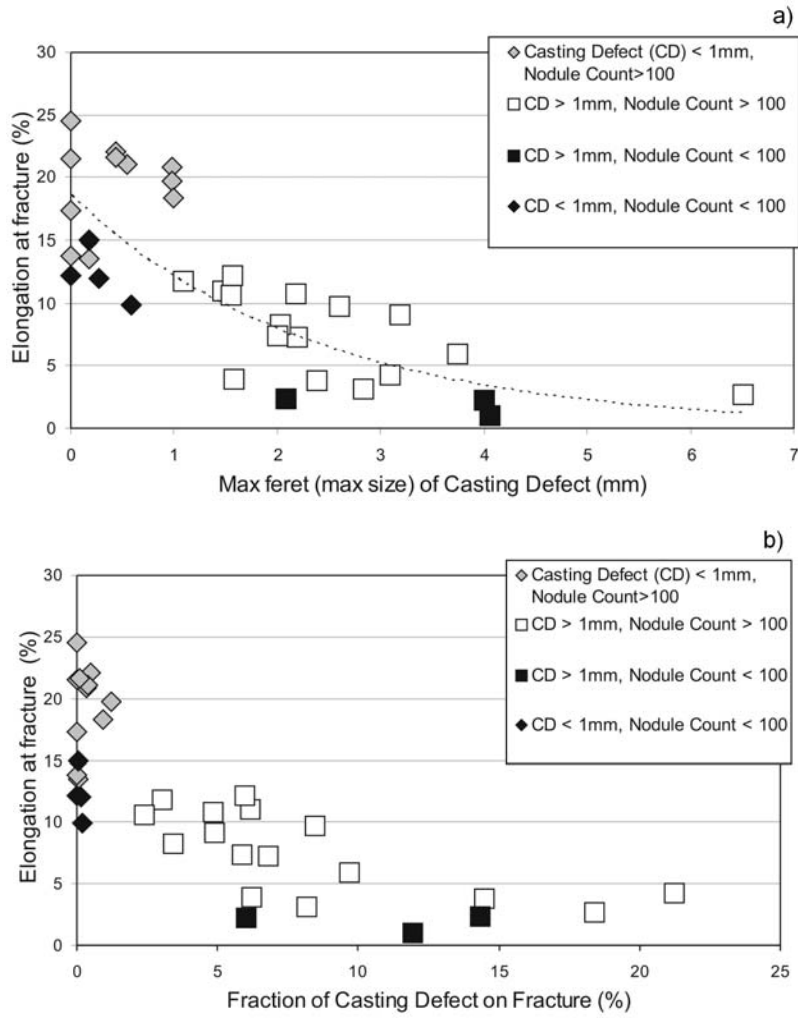


Fig. 11. Elongation at fracture versus a) maximum size of casting defect, b) area fraction of casting defects.

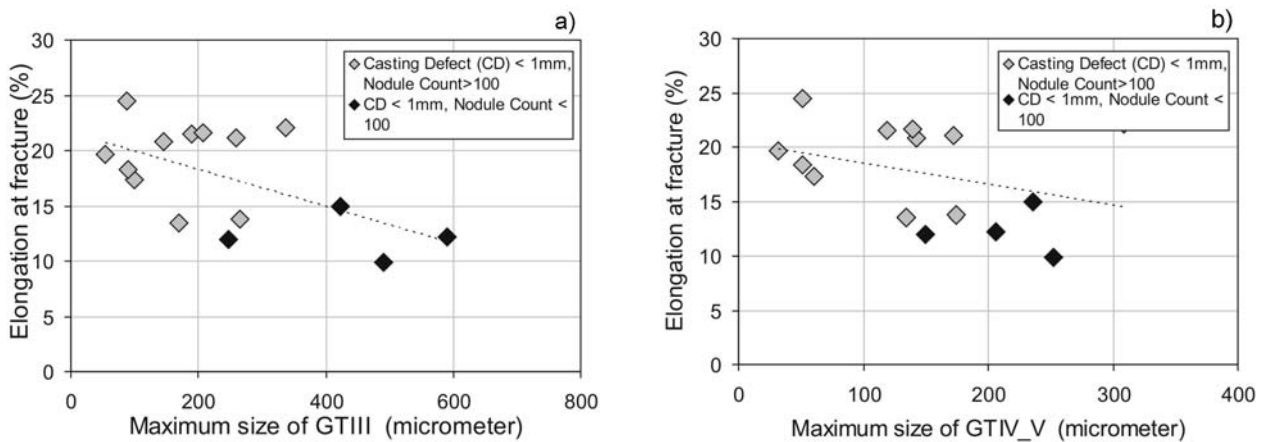


Fig. 12. The elongation at fracture versus a) GT III and b) GT IV-V maximum feret size.

In an industrial application it is important to have fast and reliable methods to verify that the graphite structure falls within the requirements. Therefore image analysis software was used. Results were com-

pared with previous work done on the same material. Seven of the specimens with defects larger than 1 mm investigated in current study had also been examined “manually” in previous investigations. By comparing

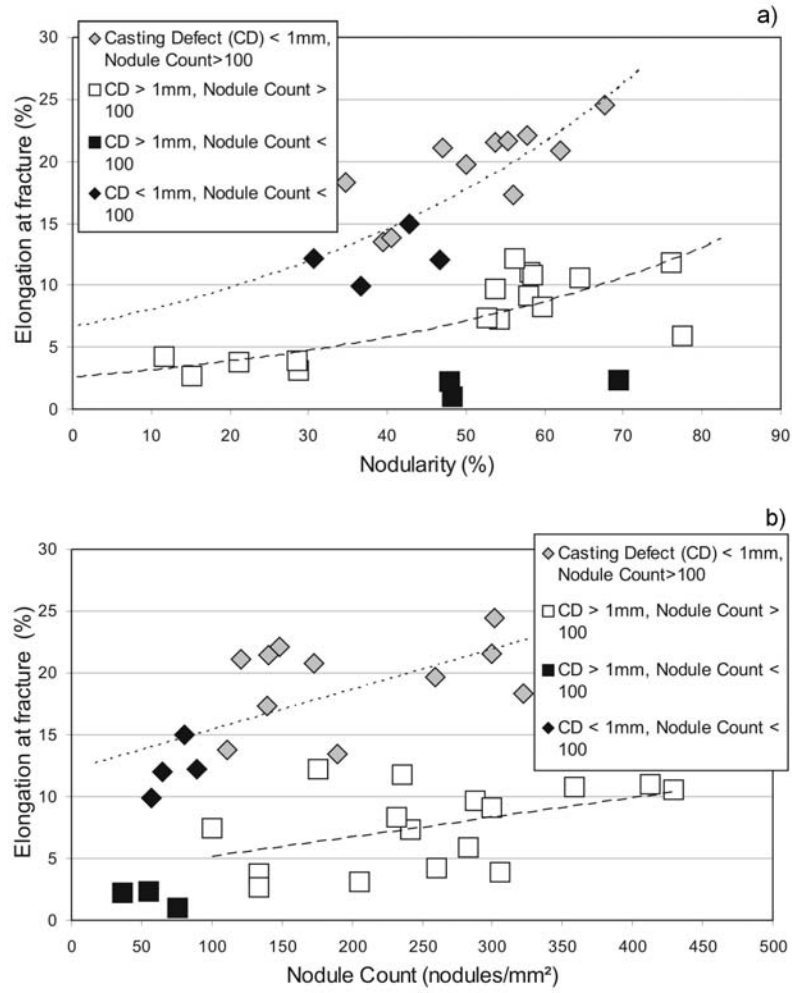


Fig. 13. Elongation at fracture versus a) nodularity and b) nodule count for casting defects smaller and larger than 1 mm, respectively.

the sizing for these seven specimens it follows that the manual sizing overestimated the defect size with an error factor ranging from 1 to 2 (Fig. 14). The probabilistic analysis in previous work computed the ductility distribution quite well but underestimated the maximum size of the defects measured in the same work [4]. One reason was that all defects were conservatively assumed to be penny-shaped, but the manual defect sizing contributed also to the discrepancy between test and analysis. Graphite nodule analysis in prepared segments had only been performed in the previous study for two of the specimens reported here. For these specimens the nodularity was significantly higher with the manual measurements. This is also expected since it is very difficult to distinguish between the Graphite Types V and VI manually and both were mostly considered as GT VI in previous study. The nodularity was therefore higher with a manual estimate.

The image processing tool that has been presented in this paper could be a very useful tool if further developed. The variation in ductility is affected by a

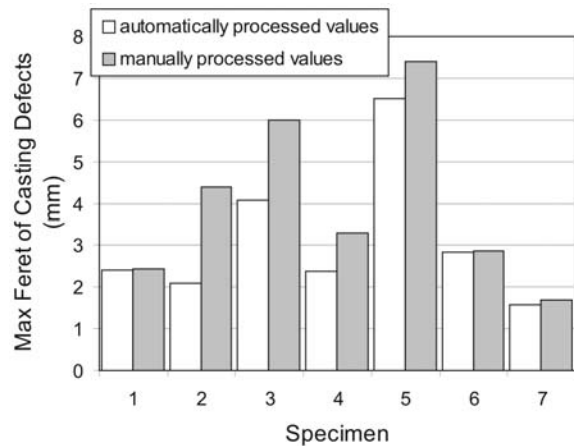


Fig. 14. Automatically acquired maximum feret values of casting defects (empty bars) for 7 samples in this study compared to maximum feret values (filled bars) from previous study, which were manually acquired.

multitude of combinations of complex and interacting microstructural features. A large number of data from different cast components are therefore needed to establish the trends reported here. The image processing tool is suitable for such analysis.

Oxide film defects can be modelled using fracture mechanics [5] and statistical distributions of the ductility can be modelled by probabilistic fracture mechanics (provided of course that these defects control ductility). The idea is to further develop such models to also include other microstructural features that affect ductility such as the nodular properties. First semi-empirical relations between elongation at fracture and each important defects/features as those outlined in this paper (maximum feret, nodularity and nodule count) need to be determined. The elongation at fracture can then be computed from the knowledge of the microstructure and checking which defect/feature is the most critical one. The inverse problem, where the microstructure in a statistical sense is computed from the statistical distribution of elongation from tensile tests, would be significantly more complex but still possible.

## 6. Conclusions

The following observations can be derived from the study presented in this article:

1. The image-processing tool presented in this paper can characterize casting defects and nodule properties in a fast and reliable way.
2. The variation in the material ductility was caused mainly by the presence of the casting defects. Casting defects present were described as blowholes, Mg-Si-Fe oxide films and thin graphite films.
3. The morphology of the graphite nodules influenced the ductility. The more the nodules deviated from their ideal spherical shape the lower was the ductility. This can be quantified in terms of increase of Graphite Type GT III and GT IV-V or reduced nodularity. A higher nodule count had also a beneficial effect on the ductility.
4. The empirical relations between elongation at fracture and casting defects and graphite nodule properties can be used to derive models for simulating variation in ductility in ductile cast iron. The casting defects can be modelled using fracture mechanics

whereas a first attempt to account for variations in graphite nodules in a first step would be based on empirical relations as those presented in this paper.

## Acknowledgements

The authors would like to acknowledge the contribution from P. Moretto for support in image analysis. This work was done as part of the JRC – Institutional Action “SAFEWASTE”.

## References

- [1] ANDERSSON, C. G.: Development of Fabrication Technology for Copper Canisters with Cast Inserts – Status Report. SKB Technical Report TR-02-07, Swedish Nuclear Fuel and Waste Management Company 2002 (available on line [www.skb.se](http://www.skb.se)).
- [2] ANDERSSON, C. G. et al.: Probabilistic Analysis and Material Characterization of Canister Inserts for Spent Nuclear Fuel – Summary Report. SKB Technical Report TR-05-17, Swedish Nuclear Fuel and Waste Management Company 2005 (available on line [www.skb.se](http://www.skb.se)).
- [3] NILSSON, K. F.—DILLSTRÖM, P.—ANDERSSON, C. G.—NILSSON, F.—ANDERSSON, M.—MINNEBO, P.—BJÖRKEGREN, L. E.—ERIXON, B.: A Probabilistic Methodology to Determine Failure Probabilities and Acceptance Criteria for the KBS-3 Inserts Under Ice-age Load Conditions, to appear in Nuclear Technology (in press).
- [4] MINNEBO, P.—NILSSON, K. F.—BLAGOEVA, D.: Journal of Materials Engineering and Performance, 16, 2007, p. 35.
- [5] NILSSON, K. F.—BLAGOEVA, D.—MORETTO, P.: Engineering Fracture Mechanics, 73, 2006, p. 1133.
- [6] EN1563-1997, Founding – Spherical Graphite Cast Irons, European Committee for Standardization.
- [7] ISO 945: Designation of Microstructure of Cast Irons – Part 1: Graphite Classification by Visual Analysis (ISO/DIS 945-1:2006), European Committee for Standardization.
- [8] EN10002-1:1990: Tensile Testing of Metallic Material – Part 1: Method of Test at Ambient Temperature, European Committee for Standardization.
- [9] VELICHKO, A.—MUCKLICH, F.: Practical Metallography, 43, 2006, p. 192.
- [10] ROWLEY, T. M.: International Atlas of Casting Defects. Schaumburg, Illinois, American Foundrymen’s Society 1993.